Models of the Membrane-Bound Cytochromes: Mössbauer Spectra of Crystalline Low-Spin Ferriheme Complexes Having Axial Ligand Plane Dihedral Angles Ranging from 0° to 90°

ARTICLE *in* JOURNAL OF THE AMERICAN CHEMICAL SOCIETY · MARCH 2006

Impact Factor: 12.11 · DOI: 10.1021/ja056343k · Source: PubMed

9 AUTHORS, INCLUDING:

Liliya A Yatsunyk
Swarthmore College
36 PUBLICATIONS **1,050** CITATIONS
SEE PROFILE

Hauke Paulsen
Universität zu Lübeck
51 PUBLICATIONS **835** CITATIONS
SEE PROFILE

W. Robert Scheidt
University of Notre Dame
363 PUBLICATIONS **13,272** CITATIONS
SEE PROFILE

F(rances) Ann Walker
The University of Arizona
240 PUBLICATIONS **8,646** CITATIONS
SEE PROFILE

J|A|C|S
ARTICLES
Published on Web 01/04/2006

Models of the Membrane-Bound Cytochromes: Mössbauer Spectra of Crystalline Low-Spin Ferriheme Complexes Having Axial Ligand Plane Dihedral Angles Ranging from 0° to 90°

Thomas Teschner,[‡] Liliya Yatsunyk,[†] Volker Schünemann,*[,‡,||] Hauke Paulsen,[‡] Heiner Winkler,[‡] Chuanjiang Hu,[#] W. Robert Scheidt,[#] F. Ann Walker,*[,†] and Alfred X. Trautwein*[,‡]

Contribution from the Institut für Physik, Universität zu Lübeck, Ratzeburger Allee 160 D-23538 Lübeck, Germany, Department of Chemistry, The University of Arizona, Tucson, Arizona 85721-0041, Fachbereich Physik, Technische Universität Kaiserslautern, Erwin-Schrödinger-Strasse 56, D-67663 Kaiserslautern, Germany, and Department of Chemistry and Biochemistry, University of Notre Dame, Notre Dame, Indiana 46556-5670

Received September 14, 2005; E-mail: awalker@u.arizona.edu; schuene@physik.uni-kl.de; trautwein@physik.uni-luebeck.de

Abstract: Crystalline samples of four low-spin Fe(III) octaalkyltetraphenylporphyrinate and two low-spin Fe(III) tetramesitylporphyrinate complexes, all of which are models of the bis-histidine-coordinated cytochromes of mitochondrial complexes II, III, and IV and chloroplast complex b_6f, and whose molecular structures and EPR spectra have been reported previously, have been investigated in detail by Mössbauer spectroscopy. The six complexes and the dihedral angles between axial ligand planes of each are [(TMP)Fe(1-MeIm)$_2$]ClO$_4$ (0°), *paral*-[(OMTPP)Fe(1-MeIm)$_2$]Cl (19.5°), *paral*-[(TMP)Fe(5-MeHIm)$_2$]ClO$_4$ (26°, 30° for two molecules in the unit cell whose EPR spectra overlap), [(OETPP)Fe(4-Me$_2$NPy)$_2$]Cl (70°), *perp*-[(OETPP)Fe(1-MeIm)$_2$]Cl (73°), and *perp*-[(OMTPP)Fe(1-MeIm)$_2$]Cl (90°). Of these, the first three have been shown to exhibit normal rhombic EPR spectra, each with three clearly resolved *g*-values, while the last three have been shown to exhibit "large g_{max}" EPR spectra at 4.2 K. It is found that the hyperfine coupling constants of the complexes are consistent with those reported previously for low-spin ferriheme systems, with the largest-magnitude hyperfine coupling constant, A_{zz}, being considerably smaller for the "parallel" complexes (400−540 kG) than for the strictly perpendicular complex (902 kG), A_{xx} being negative for all six complexes, and A_{zz} and A_{xx} being of similar magnitude for the "parallel" complexes (for example, for [(TMP)Fe(1-MeIm)$_2$]Cl, $A_{zz} = 400$ kG, $A_{xx} = -400$ kG). In all cases, A_{yy} is small but difficult to estimate with accuracy. With results for six structurally characterized model systems, we find for the first time qualitative correlations of g_{zz}, A_{zz}, and ΔE_Q with axial ligand plane dihedral angle $\Delta\varphi$.

Introduction

Heme-containing electron-transfer proteins are essential to many biological processes. The two major classes of heme-based electron-transport proteins, having bis-histidine- and histidine-methionine-coordinated heme centers, shuttle between iron(II) and iron(III) oxidation states and are usually called the cytochromes *a*, *b*, and *c*, based on the differing substituents on the periphery of the heme. In addition to relatively small molecular weight heme proteins,[1−9] a number of cytochrome-containing multi-heme protein complexes with bis-histidine coordination are known. These include the cytochromes *b* of mitochondrial Complexes II,[10] III,[11−25] and chloroplasts[26−29] and the cytochrome *a* of mitochondrial Complex IV (cytochrome

[‡] Universität zu Lübeck.
[†] The University of Arizona.
[||] Technische Universität Kaiserslautern.
[#] University of Notre Dame.

(1) Mathews, F. S.; Czerwinski, E. W.; Argos, P. In *The Porphyrins*; Dolphin, D., Ed; Academic Press: New York, 1979; Vol. VII, pp 108−147.
(2) Lederer, F.; Ghrir, R.; Guiard, B.; Cortial, S.; Ito, A. *Eur. J. Biochem.* **1983**, *132*, 95−102.
(3) Pierrot, M.; Haser, R.; Frey, M.; Payan, F.; Astier, J.-P. *J. Biol. Chem.* **1982**, *257*, 14341−14348.
(4) Higuchi, Y.; Kusunoki, M.; Matsuura, Y.; Yasuoka, N.; Kakudo, M. *J. Mol. Biol.* **1984**, *172*, 109−139.
(5) Simões, P.; Matias, P. M.; Morais, J.; Wilson, K.; Dauter, Z.; Carrondo, M. A. *Inorg. Chim. Acta* **1998**, *273*, 213−224.
(6) Nørager, S.; Legrand, P.; Pieulle, L.; Hatchikian, C.; Roth, M. *J. Mol. Biol.* **1999**, *290*, 881−902.
(7) Brennan, L.; Turner, D. L.; Fareleira, P.; Santos, H. *J. Mol. Biol.* **2001**, *308*, 353−365.
(8) Hamada, K.; Bethge, P. H.; Mathews, F. S. *J. Mol. Biol.* **1995**, *247*, 947−962.
(9) Timkovich, R. In *The Porphyrins*; Dolphin, D., Ed.; Academic Press: New York, 1979; Vol. 12, pp 241−294.
(10) Sun, F.; Huo, X.; Zhai, Y.; Wang, A.; Xu, J.; Su, D.; Bartiam, M.; Rao, Z. *Cell* **2005**, *121*, 1043−1067.
(11) Xia, D.; Yu, C.-A.; Kim, H.; Xia, J.-Z.; Kachurin, A. M.; Zhang, L.; Yu, L.; Deisenhofer, J. *Science* **1997**, *277*, 60−66.
(12) Iwata, S.; Lee, J. W.; Okada, K.; Lee, J. K.; Iwata, M.; Rasmussen, B.; Link, T. A.; Ramaswamy, S.; Jap, B. K. *Science* **1998**, *281*, 64−71.
(13) Zhang, Z.; Huang, L.; Shulmeister, V. M.; Chi, Y.-I.; Kim K. K.; Hung, L.-W.; Crofts, A. R.; Berry, E. A.; Kim, S.-H. *Nature* **1998**, *392*, 677−684.
(14) Berry, E. A.; Huang, L.-S.; Zhang, Z.; Kim, S.-H. *J. Bioenerg. Biomembr.* **1999**, *31*, 177−190.
(15) Yu, C.-A.; Tian, H.; Zhang, L.; Deng, K.-P.; Shenoy, S. K.; Yu, L.; Xia, D.; Kim, H.; Deisenhofer, J. *J. Bioenerg. Biomembr.* **1999**, *31*, 191−199.
(16) Berry, E. A.; Guergova-Kuras, M.; Huang, L.; Crofts, A. R. *Annu. Rev. Biochem.* **2000**, *69*, 1005−1075.

oxidase),[30] as well as bacterial analogues of these multi-heme electron-transfer proteins and a number of additional multi-heme cytochromes *c* that are involved in electron transfer and/or redox of the oxides of nitrogen,[31−34] sulfur,[35] and other main group elements. Complex III, also called the cytochrome bc_1 complex or ubiquinol:cytochrome *c* oxidoreductase, plays an important role in the electron transfer in mitochondria, chloroplasts, and many aerobic and photosynthetic bacteria. It transfers electrons from the lipophilic ubiquinol (a two-electron donor), which was pre-reduced by mitochondrial Complex II, to soluble cytochrome *c*, a one-electron acceptor; this process is coupled to translocation of two protons across the inner mitochondrial membrane per two electrons passed to cytochrome *c*, which then carries them, one at a time, to cytochrome oxidase (Complex IV).[29] Cytochrome b_6f of photosynthetic bacteria and chloroplasts transfers electrons from the lipophilic plastoquinol (a two-electron donor), which was pre-reduced by Photosystem II, to a hydrophilic one-electron acceptor (a *c*-type cytochrome for photosynthetic bacteria or plastocyanin for chloroplasts), which then reduces Photosystem I, and couples this electron transfer to translocation of two protons across the chloroplast membrane.[36] The characterization and mechanistic understanding of these high-molecular-weight, membrane-bound, multi-heme systems continues to be a significant challenge.

One of the first and most useful spectroscopic tools that provided much insight into the number, properties, and roles of the heme centers in the cytochrome bc_1 complex was EPR spectroscopy. The unusual EPR spectra for the cytochrome bc_1 complex were first reported by Orme-Johnson, Hansen, and Beinert[37] and later analyzed in detail by Salerno.[38] EPR data for the bc_1 complex show that both of the *b* hemes (as well as the c_1 heme) exhibit the single-feature EPR signals known as highly anisotropic low-spin (HALS) or, preferably, "large g_{max}"[39] type with $g_{max} = 3.41-3.44$ and $3.75-3.78$ for high and low reduction potential hemes, b_H and b_L, respectively. Cytochrome b_6f does not yield a resolved EPR signal for the hemes of cytochrome b_6 (except for the high-spin heme sometimes called heme x[40]), but the *g*-values of hemes b_l and b_h (also called b_n and b_p) have been estimated as 3.6 by magnetic Mössbauer spectroscopy.[41] For the cytochrome bc_1 complex of mitochondria and the structurally and functionally related cytochrome b_6f complex of chloroplasts, these "large g_{max}" EPR signals "relax" to normal rhombic EPR signals (with g_1, g_2, and g_3 values observed, and typically 2.9, 2.25, and 1.54, respectively) when the cytochrome *b* protein is extracted from the membrane and the other proteins of the complex.[42−44]

In earlier work with bis-imidazole-ligated iron(III) porphyrinates, we have found that the axial ligand arrangement, i.e., the absolute and relative orientations of the two planar axial ligands, is an important factor in defining the EPR spectroscopic properties.[39,45−48] Ligand orientation is also likely to be a significant determinant of the reduction potentials of these heme centers. Studies with synthetic ferriheme complexes have shown that the coordination of bulky imidazoles (2-methylimidazole, 1,2-dimethylimidazole, etc.) or some pyridines (3,4-dimethylamino-pyridine, pyridine itself, etc.) to iron(III) tetraphenylporphyrin (TPPFe(III))[39,45] or hemin itself ((ProtoIX)Fe(III))[49,50] leads to a "large g_{max}" EPR signal similar to that reported for the bc_1 complex.[37,38] These signals have one *g* value ≥3.2 (sometimes as large as 3.78) and nearly or completely undetectable g_2 and g_3, and are observable only at very low temperature (<10 K in most cases).[49] A "large g_{max}" EPR signal was first shown by Walker, Scheidt, and their co-workers to occur for ferriheme complexes with a $(d_{xy})^2(d_{xz},d_{yz})^3$ electronic ground state in which the splitting between the d_{xz} and d_{yz} orbitals is small (usually less than the value of the spin−orbit coupling constant, λ, or <400 cm^{-1}).[39,47,51,52] This is the case where axial ligands are in perpendicular planes[39,51] or where ligands without planes are used (e.g., CN^-,[46,53] phosphines,[51] NH_3,[51] or alkylamines, as in cytochrome f[54]). On the other hand, normal rhombic EPR signals are observed when the splitting between the d_{xz} and d_{yz} orbitals is larger, on the order of 2−3 times the spin−orbit coupling constant, λ, or 600−1200 cm^{-1}.[39,47,51] In this case, planar axial ligands coordinated to iron are oriented in parallel planes. Hence, the first correlation of structure with

(17) Gao, X.; Wen, X.; Yu, C.; Esser, L.; Tsao, S.; Quinn, B.; Zhang, L.; Yu, L.; Xia, D. *Biochemistry* **2002**, *41*, 11692−11702.
(18) Gao, X.; Wen, X.; Esser, L.; Quinn, B.; Yu, L.; Yu, C.-A.; Xia, D. *Biochemistry* **2003**, *42*, 9067−9080.
(19) Huang, L.; Cobessi, D.; Tung, E. Y.; Berry, E. A. *J. Mol. Biol.* **2005**, *351*, 573−597.
(20) Crofts, A. R. *Annu. Rev. Physiol.* **2004**, *66*, 689−733.
(21) Hunte, C.; Koepke, J.; Lange, C.; Rossmanith, T.; Michel, H. *Structure* **2000**, *8*, 669−684.
(22) Lange, C.; Nett, J. H.; Trumpower, B. L.; Hunte, C. *EMBO J.* **2001**, *20*, 6591−6600.
(23) Lange, C.; Hunte, C. *Proc. Natl. Acad. Sci. U.S.A.* **2002**, *99*, 2800−2805.
(24) Palsdottir, H.; Lojero, C. G.; Trumpower, B. L.; Hunte, C. *J. Biol. Chem.* **2003**, *278*, 31303−31311.
(25) Berry, E. A.; Huang, L.-S.; Saechao, L. K.; Pon, N. G.; Valkova-Valchanova, M.; Daldal, F. *Photosynth. Res.* **2004**, *81*, 251−275.
(26) Stroebel, D.; Choquet, Y.; Popot, J.-L.; Picot, D. *Nature* **2003**, *426*, 413−418.
(27) Durisu, G.; Zhang, H.; Smith, J. L.; Cramer, W. A. *Science* **2003**, *302*, 1009−1014.
(28) Cramer, W. A.; Zhang, H.; Yan, J.; Kurisu, G.; Smith, J. L. *Biochemistry* **2004**, *43*, 5921−5929.
(29) Smith, J. L.; Zhang, H.; Yan, J.; Kurisu, G.; Cramer, W. A. *Curr. Opin. Struct. Biol.* **2004**, *14*, 432−439.
(30) Michel, H.; Behr, J.; Harrenga, A.; Kannt, A. *Annu. Rev. Biophys. Biomol. Struct.* **1998**, *27*, 329−356.
(31) Einsle, O.; Messerschmidt, A.; Stach, P.; Bourenkov, G. P.; Bartunik, H. D.; Huber, R.; Kroneck, P. M. H. *Nature* **1999**, *400*, 476−480.
(32) Einsle, O.; Stach, P.; Messerschmidt, A.; Simon, J.; Kröger, A.; Huber, R.; Kroneck, P. M. H. *J. Biol. Chem.* **2000**, *275*, 39608−39616.
(33) Jafferji, A.; Allen, J. W. A. Ferguson, J. J.; Fülöp, V. *J. Biol. Chem.* **2000**, *275*, 25089−25094.
(34) Jormakka, M.; Törnroth, S.; Byrne, B.; Iwata, S. *Science* **2002**, *295*, 1863−1868.
(35) Crane, B. R.; Siegel, L. M.; Getzoff, E. D. *Science* **1995**, *270*, 59−67.
(36) Breyton, C. *Biochim. Biophys. Acta* **2000**, *1459*, 467−474.
(37) Orme-Johnson, N. R.; Hansen, R. E.; Beinert, H. *Biochem. Biophys. Res. Commun.* **1974**, *45*, 871−878.
(38) Salerno, J. C. *J. Biol. Chem.* **1984**, *259*, 2331−2336.
(39) Walker, F. A.; Huynh, B. H.; Scheidt, W. R.; Osvath, S. R. *J. Am. Chem. Soc.* **1986**, *108*, 5288−5297.
(40) Zhang, H.; Primak, A.; Cape, J.; Bowman, M. K.; Kramer, D. M.; Cramer, W. A. *Biochemistry* **2004**, *43*, 16329−16336.
(41) Schünemann, V.; Trautwein, A. X.; Illerhaus, J.; Haehnel, W. *Biochemistry* **1999**, *38*, 8981−8991.
(42) T'sai, A.-L.; Palmer, G. *Biochim. Biophys. Acta* **1982**, *681*, 484−495.
(43) Salerno, J. C.; McGill, J. W.; Gerstle, G. C. *FEBS Lett.* **1983**, *162*, 257.
(44) Salerno, J. C.; Yoshida, S.; King, T. E. *J. Biol. Chem.* **1986**, *261*, 5480−5486.
(45) Walker, F. A.; Reis, D.; Balke, V. L. *J. Am. Chem. Soc.* **1984**, *106*, 6888−6898.
(46) Innis D.; Soltis, S. M.; Strouse, C. E. *J. Am. Chem. Soc.* **1988**, *110*, 5644−5650.
(47) Walker, F. A. *Coord. Chem. Rev.* **1999**, *185−186*, 471−534.
(48) Walker, F. A. *Chem. Rev.* **2004**, *104*, 589−615.
(49) Carter, K. R.; T'sai, A.-L.; Palmer, G. *FEBS Lett.* **1981**, *132*, 243−246.
(50) Migita, C. T.; Iwaizumi, M. *J. Am. Chem. Soc.* **1981**, *103*, 4378−4381.
(51) Scheidt, W. R.; Kirner, J. F.; Hoard, J. L.; Reed, C. A. *J. Am. Chem. Soc.* **1987**, *109*, 1963−1968.
(52) Walker, F. A. In *The Porphyrin Handbook*; Kadish, K. M., Smith, K. M., Guilard, R., Eds.; Academic Press: San Diego, CA, 2000; Chapter 36, Vol. 5, pp 81−183.
(53) Ikeue, T.; Ohgo, Y.; Saitoh, T.; Yamaguchi, T.; Nakamura, M. *Inorg. Chem.* **2001**, *40*, 3423−3434.
(54) Martinez, S. E.; Huang, D.; Ponomarev, M.; Cramer, W. A.; Smith, J. L. *Protein Sci.* **1996**, *5*, 1081−1092.

EPR spectral type was established: "large g_{max}" spectra indicate axial ligands in perpendicular planes, while normal rhombic spectra indicate axial ligands in parallel planes.[48]

The systems investigated as models of the bis-histidine-coordinated cytochromes have all utilized synthetic hemes such as octaethylporphyrinatoiron(III)/(II), (OEP)Fe, tetraphenylporphyrinatoiron(III)/(II), (TPP)Fe, or other tetraarylporphyrin-type systems such as tetramesitylporphyrinatoiron(III)/(II), (TMP)Fe,[47,51,55−57] and, more recently, octaalkyltetraphenylporphinatoiron(III), (OETPP)Fe, (OMTPP)Fe, and (TC_6TPP)-Fe,[48,58,59] in each case with two imidazole or high-basicity pyridine axial ligands. Knowledge from these model heme systems has been applied to the interpretation of the structure and function of the heme proteins such as the cytochrome-containing systems of Complexes II and III of inner mitochondrial membranes. At the highest resolution obtained thus far (2.1 Å),[60] the bovine cytochrome bc_1 complex structure has the two *b* heme centers with axial histidine imidazole plane dihedral angles of 86° and 64°; the yeast structure, with highest resolution 2.3 Å,[23,24] has those same angles as 84° and 71°. Among 10 recent structures from bovine, avian, yeast, and bacterial bc_1 complexes, the average angles are 84° ± 4° and 60° ± 7° for hemes b_L and b_H, respectively.[13,14,17−19,21,22,24,25,60] The larger-dihedral angle heme center, b_L, has been assigned the EPR signal with $g_{max} = 3.75-3.78$, and the smaller-dihedral angle one, b_H, has been assigned the EPR signal with $g_{max} = 3.41-3.44$ on the basis of EPR spectra obtained during redox titrations.[38,61] Reduction potentials for the b_L and b_H centers of murine Complex III are −31 ± 12 and +92 ± 14 mV, respectively,[62] and those for other mammalian *b* heme centers are similar, but all are affected by the conditions used for measurements, including detergent or lipid and the electron-transfer mediators used, as well as the presence of inhibitors that bind to the quinone sites and the state of oxidation of the quinone near heme b_H.[63]

Mössbauer spectroscopy is another technique that has been utilized to characterize some ferriheme protein systems,[41,64−70] but no investigations of the mitochondrial Complexes II, III and IV have yet been reported. The magnetic Mössbauer spectra of several multi-heme protein complexes have been reported,[41,68,70] although it is very difficult to deconvolute the overlapping Mössbauer spectra of multi-heme complexes when the parameters of the centers are similar. Therefore, investigations of synthetic ferriheme models by Mössbauer spectroscopy can be helpful in interpreting the complex patterns observed for multi-heme complexes. The magnetic Mössbauer spectra of some OEP, TPP, TMP, and other phenyl-substituted TPP complexes of Fe(III)[39,56,71−73] and Fe(II)[74−76] have been reported previously. These studies have clearly shown that the Mössbauer quadrupole splittings in small applied magnetic field are sensitive to the axial ligand orientation,[39,56,71−73] and at least the broad categories of "parallel" and "perpendicular" relative ligand orientation can be distinguished. Furthermore, by fitting the magnetic Mössbauer spectra, the two unobserved *g*-values in the EPR spectra of "large g_{max}" centers can be estimated.[39,56,71−73] However, while the largest hyperfine coupling constant, A_{zz}, can be estimated very accurately from the spread of the magnetic Mössbauer spectrum, the two smaller-magnitude hyperfine coupling constants, A_{yy} and A_{xx}, are usually less accurately determined by the spectral fits,[73] and thus the values of the other two *g*-values, g_{yy} and g_{xx}, usually cannot be as well defined as desired. Furthermore, from magnetic Mössbauer and EPR spectra alone, it is sometimes not possible to determine unambiguously whether g_{zz} or g_{xx} is the largest *g*-value, and thus it cannot be stated with certainty whether the unpaired electron is in the d_{yz} or the d_{xy} orbital, respectively.[73] In these cases (where the rhombicity, V/Δ, is greater than 2/3), single-crystal EPR data or pulsed EPR data on frozen solution samples are required to determine the orientation of the **g**-tensor and thus whether the electron configuration is $(d_{xy})^2(d_{xz},d_{yz})^3$ or $(d_{xz},d_{yz})^4(d_{xy})^1$.[72,77−81] However, this is not a problem for bis-histidine-coordinated cytochromes and their models, which have all long been known to have $(d_{xy})^2(d_{xz},d_{yz})^3$ electron configurations,[37−39,46,77,78,80,82−85,89] and thus for all of these systems the Mössbauer spectra can be unambiguously interpreted in terms of the latter electron configuration.

(55) Safo, M. K.; Gupta, G. P.; Walker, F. A.; Watson, C. T.; Simonis, U.; Scheidt, W. R. *J. Am. Chem. Soc*. **1992**, *114*, 7066−7075.
(56) Safo, M. K.; Gupta, G. P.; Walker, F. A.; Scheidt, W. R. *J. Am. Chem. Soc*. **1991**, *113*, 5497−5510.
(57) Munro, O. Q.; Serth-Guzzo, J. A.; Turowska-Tyrk, I.; Mohanrao, K.; Shokhireva, T. Kh.; Walker, F. A.; Debrunner, P. G.; Scheidt, W. R. *J. Am. Chem. Soc.* **1999**, *121*, 11144−11155.
(58) Ogura, H.; Yatsunyk, L.; Medforth, C. J.; Smith, K. M.; Barkigia, K. M.; Renner, M. W.; Melamed, D.; Walker, F. A. *J. Am. Chem. Soc.* **2001**, *123*, 6564−6578.
(59) Yatsunyk, L.; Carducci, M. D.; Walker, F. A. *J. Am. Chem. Soc.* **2003**, *125*, 15986−16005.
(60) Protein Data Bank filename 2A06, deposited June 2005.
(61) Schütz, M.; Schoepp-Cothenet, B.; Lojou, E.; Woodstra, M.; Lexa, D.; Tron, P.; Dolla, A.; Durand, M.-C.; Stetter, K. O.; Baymann, F. *Biochemistry* **2003**, *42*, 10800−10808.
(62) Howell, N.; Robertson, D. E. *Biochemistry* **1993**, *32*, 11162−11172.
(63) Salerno, J. C.; Xu, Y.; Osgood, M. P.; Kim, C. H.; King, T. E. *J. Biol. Chem.* **1989**, *264*, 15398−15403.
(64) Sharrock, M.; Debrunner, P. G.; Schulz, C.; Lipscomb, J. D.; Marshall, V.; Gunsalus, I. C. *Biochim. Biophys. Acta* **1976**, *420*, 8−26.
(65) Huynh, B. H.; Emptage, M. H.; Münck, E. *Biochim. Biophys. Acta* **1978**, *534*, 295−306.
(66) Dwivedi, A.; Toscano, W. A.; Debrunner, P. G. *Biochim. Biophys. Acta* **1979**, *576*, 502−508.
(67) Rhynard, D.; Lang, G.; Spartalian, K.; Yonetani, T. *J. Chem. Phys.* **1979**, *71*, 3715−3721.
(68) Huynh, B. H.; Lui, M. C.; Moura, J. J. G.; Moura, I.; Ljungdahl, P. O.; Münck, E.; Payne, W. J.; Peck, H. D.; DerVartanian, D. V.; LeGall, J. *J. Biol. Chem.* **1982**, *257*, 9576−9581.
(69) Debrunner, P. G. In *Iron Porphyrins*; Lever, A. B. P., Gray, H. B., Eds.; VCH: Weinheim, Germany, 1989; Part 3, pp 137−227.
(70) Costa, C.; Moura, J. J. G.; Moura, I.; Liu, M. Y.; Peck, H. D.; LeGall, J.; Wang, Y.; Huynh, B. H. *J. Biol. Chem.* **1990**, *265*, 14382−14387.
(71) Schünemann, V.; Raitsimring, A. M.; Benda, R.; Trautwein, A. X.; Shokhireva, T. Kh.; Walker, F. A. *J. Biol. Inorg. Chem.* **1999**, *4*, 709−716.
(72) Benda, R.; Schünemann, V.; Trautwein, A. X.; Walker, F. A. *Isr. J. Chem.* **2000**, *40*, 9−14.
(73) Benda, R.; Schünemann, V.; Trautwein, A. X.; Cai, S.; Polam, J. R.; Watson, C. T.; Shokhireva, T. Kh.; Walker, F. A. *J. Biol. Inorg. Chem.* **2003**, *42*, 787−801.
(74) Polam, J. R.; Wright, J. L.; Christensen, K. A.; Walker, F. A.; Flint, H.; Winkler, H.; Grodzicki, M.; Trautwein, A. X. *J. Am. Chem. Soc.* **1996**, *118*, 5272−5276.
(75) Grodzicki, M.; Flint, H.; Winkler, H.; Walker, F. A.; Trautwein, A. X. *J. Phys. Chem. A* **1997**, *101*, 4202−4207.
(76) Hu, C.; Noll, B. C.; Schulz, C. E.; Scheidt, W. R. *Inorg. Chem.* **2005**, *44*, 4346−4358.
(77) Raitsimring, A. M.; Borbat, P.; Shokhireva, T. Kh.; Walker, F. A. *J. Phys. Chem.* **1996**, *100*, 5235−5244.
(78) Raitsimring, A. M.; Walker, F. A. *J. Am. Chem. Soc.* **1998**, *120*, 991−1002.
(79) Simonneaux, G.; Schünemann, V.; Morice, C.; Carel, L.; Toupet, L.; Winkler, H.; Trautwein, A. X.; Walker, F. A. *J. Am. Chem. Soc.* **2000**, *122*, 4366−4377.
(80) Astashkin, A. V.; Raitsimring, A. M.; Walker, F. A. *J. Am. Chem. Soc.* **2001**, *123*, 1905−1913.
(81) Rivera, M.; Caignan, G. A.; Astashkin, A. V.; Raitsimring, A. M.; Shokhireva, T. Kh.; Walker, F. A. *J. Am. Chem. Soc.* **2002**, *124*, 6077−6089.
(82) Blumberg, W. E.; Peisach, J. *Adv. Chem. Ser.* **1971**, *100*, 271−291.
(83) Peisach, J.; Blumberg, W. E.; Adler, A. D. *Ann. N.Y. Acad. Sci.* **1973**, *206*, 310−327.
(84) Taylor, C. P. S. *Biochim. Biophys. Acta* **1977**, *491*, 137−149.
(85) Palmer, G. *Biochem. Soc. Trans.* **1985**, *13*, 548−560.

In previous studies from this laboratory, Mössbauer spectra of bis-imidazole or -pyridine complexes of iron(III) porphyrinates were obtained for ^{57}Fe-enriched frozen solution or rapidly precipitated polycrystalline samples,[71−73] and it was found that the magnetic Mössbauer spectra were difficult to fit and appeared to consist of several overlapping spectra from species that were in some way different from each other. Thus, in this study, we have investigated the Mössbauer spectra of pure crystalline samples of the same crystalline form as that for which the crystal structure was determined, to see whether there might be a direct relationship between the axial ligand plane dihedral angle $\Delta\varphi$ and the Mössbauer parameters observed for model ferriheme complexes, and whether crystalline samples might lead to more precise fitting of the magnetic Mössbauer spectra. Accordingly, in this paper we describe the Mössbauer spectra of six crystalline complexes, [(OETPP)Fe(4-Me$_2$NPy)$_2$]$^+$, *perp*-[(OETPP)Fe(1-MeIm)$_2$]$^+$, [(TMP)Fe(1-MeIm)$_2$]$^+$, *paral*-[(TMP)-Fe(5-MeHIm)$_2$]$^+$, and two of [(OMTPP)Fe(1-MeIm)$_2$]$^+$ with different axial ligand plane dihedral angles, $\Delta\varphi$. Structural data are available for all of these complexes,[56−59] and the crystalline samples used for the Mössbauer spectral investigations utilized exactly the same crystalline form as that used for the earlier structure determinations. The axial ligand plane dihedral angles of these six complexes span the entire possible range of $\Delta\varphi$, from 0° to 90°. Three complexes display normal rhombic EPR spectra (dihedral angles 0°,[56] 19.5°[59] and 26°, 30°[57,86]); the remaining three exhibit "large g_{max}" EPR signals at 4.2 K.[58,59] These latter three complexes were the ones we were initially most interested in studying. As it turns out, all six of the complexes provided new information that is valuable to our understanding of the magnetic spectroscopic properties of these types of ferriheme systems, and the results show us clearly that the difficulties encountered previously in fitting the Mössbauer spectra of ferriheme model complexes in frozen solution or solid samples that precipitated rapidly from solution[71−73] probably arose from the presence of multiple orientations of the axial ligands within the two broad classes of ligand orientations ("parallel" and "perpendicular"). Thus, from the present work, it is clear for the first time that there are qualitative relationships between the axial ligand plane dihedral angle $\Delta\varphi$ and the largest EPR g-value, g_{zz}, the largest Mössbauer hyperfine coupling constant, A_{zz}, and, to a lesser extent, the quadrupole coupling constant, ΔE_Q.

Experimental Section

The crystalline samples of *paral*-[(TMP)Fe(5-MeHIm)$_2$]ClO$_4$, [(TMP)-Fe(1-MeIm)$_2$]ClO$_4$, *paral*-[(OMTPP)Fe(1-MeIm)$_2$]Cl, *perp*-[(OMTPP)-Fe(1-MeIm)$_2$]Cl, *perp*-[(OETPP)Fe(1-MeIm)$_2$]Cl, and [(OETPP)Fe(4-Me$_2$NPy)$_2$]Cl, whose crystal and molecular structures are known, were prepared as described previously.[56−59] Polycrystalline natural iron-containing samples for Mössbauer spectroscopy were placed in solid Delrin sample holders and covered with a minimum of mother liquor for the octaalkyltetraphenylporphyrinates, which contain solvent molecules of crystallization,[58,59] or without mother liquor for the TMP complexes, which do not.[56,57] They were cooled to 233 K during shipping and then stored at 77 K.

Mössbauer spectra were recorded using a conventional spectrometer in the constant-acceleration mode. Isomer shifts are given relative to α-Fe at room temperature. The spectra obtained at 20 mT were measured in a liquid helium bath cryostat (Oxford MD 306) equipped with a pair of permanent magnets. For the high-field spectra a cryostat equipped with a superconducting magnet was used (Oxford Instruments). Magnetically split spectra of paramagnetic samples were simulated in the spin-Hamiltonian approximation described below; otherwise, spectra were analyzed by least-squares fits using Lorentzian line shapes.

The Zeeman interaction of a spin with an applied field $\vec{B}$ and describing the electronic **g**-tensor is given by the Hamiltonian

$$\hat{H}_{el} = \mu_B \vec{S}\vec{g}\vec{B} \quad (1)$$

where μ_B denotes the Bohr magneton. Magnetic Mössbauer spectra were simulated using eq 1 together with the nuclear Hamiltonian[87]

$$\hat{H}_N = \frac{eQV_{zz}}{4I(2I-1)}[3\hat{I}_z^2 - I(I+1) + \eta(\hat{I}_x^2 - \hat{I}_y^2)] - g_N\mu_N\vec{I}\vec{B} + \langle\vec{S}\rangle\vec{A}\vec{I} \quad (2)$$

Here I denotes the nuclear spin quantum number, Q the nuclear quadrupole moment of the excited nuclear state, V_{zz} the z-component of the electric-field gradient (EFG) tensor and $\eta = (V_{xx} - V_{yy})/V_{zz}$ the asymmetry parameter of the EFG, g_N the nuclear g-factor, $\langle\vec{S}\rangle$ the electron spin expectation value, and μ_N the nuclear magneton. Note that the axis system being used for the EFG is that of the **g**- and **A**-tensors, i.e., with z along the normal to the porphyrin plane and x and y axes in the porphyrin plane.[47,48,84] The **g**-tensor normalization condition $g_{xx}^2 + g_{yy}^2 + g_{zz}^2 = 16$[84,88,89] was used in this fitting procedure.

Results and Discussion

X-band EPR spectra of all samples of this study have already been reported[56−59] and the g-values are summarized in Table 1, where x, y, and z axes are defined in terms of the molecular frame, with z oriented along the heme normal and x and y in the porphyrin plane in all cases. Field-dependent Mössbauer spectra, obtained at 4.2 K, of *perp*-[(OMTPP)Fe(1-MeIm)$_2$]Cl ($\Delta\varphi = 90°$) are shown in Figure 1. The spectrum of *perp*-[(OMTPP)Fe(1-MeIm)$_2$]Cl, recorded in the presence of a small magnetic field of 20 mT perpendicular to the γ-beam (Figure 1a) (as well as the 4.0 and 7.0 T spectra, Figure 1b,c), exhibits a magnetically split six-line pattern. Spectra acquired with the magnetic field applied parallel to the γ-beam are shown in Supporting Information Figure S1. Based upon the assumption that "g_{max}" $= g_{zz} = 3.61$, the spectra can be simulated with the following hyperfine coupling tensor elements: $A_{zz} = +902$ kG, $A_{xx} = -225$ kG, and $A_{yy} = 293$ kG (Table 1). Applying the normalization condition for the **g**-tensor ($\sum g^2 = 16$) leads to the best estimates of g_{yy} and g_{xx} of 1.53 and 0.63, respectively. These values are thus used to calculate the crystal field parameters, tetragonality and rhombicity,[84] given in Table 1.

The internal magnetic field at the ^{57}Fe nucleus is given by $\vec{H}_{int} = -\langle\vec{S}\rangle\cdot\vec{S}/g_N\mu_N$. For the magnetic splitting, the effective hyperfine field, which is the sum of the external and the internal fields, must be considered. Nevertheless, the internal field dominates strongly, and therefore the magnetic splitting of a ferric low-spin system is effectively determined by the product $\langle\vec{S}\rangle\cdot\vec{A}$. For $S = {}^1/_2$ ferric ion, the symmetry of the **g**-tensor is reflected within direction-dependent spin expectation values. The corresponding **g**-tensor component determines the sign of the

(86) Two molecules are found in the unit cell, one with an axial ligand plane dihedral angle of 26° and the other of 30°, but the two have similar angles φ from the N−Fe−N axes.[57] Although there is evidence of two overlapping EPR spectra, it was not possible to deconvolute the two because of the similarity of the g-values.[57]

(87) Trautwein, A. X.; Bill, E.; Bominaar, E. L.; Winkler, H. *Struct. Bonding* **1991**, *78*, 1−95.
(88) Oosterhuis, W. T.; Lang, G. *Phys. Rev.* **1969**, *178*, 439−456.
(89) Griffith, J. S. *Mol. Phys.* **1971**, *21*, 135−139.

Table 1. Mössbauer Data for Selected Ferriheme Complexes in This Study

complex	δ (mm/s)	ΔE_Q (mm/s)	η	V_{ii}[a] (mm/s)	**g**-tensor[b]	$A/g_N\mu_N$[c] (kG)
perp-[(OMTPP)Fe(1-MeIm)$_2$]$^+$ (90.0°)	0.27 ± 0.02 (4.2 K)	1.70 ± 0.02	−0.87 ± 0.25	$V_{xx} = -1.42$ $V_{yy} = -0.10$ $V_{zz} = 1.52$	$g_{xx} = 0.63$[d] $g_{yy} = 1.53$[d] $g_{zz} = 3.61$[e]	$A_{xx} = -225 \pm 150$ (−298) $A_{yy} = 293 \pm 30$ (163) $A_{zz} = 902 \pm 5$ (919) (crystal field $V/\lambda = 0.64$, $\Delta/\lambda = 3.82$, $V/\Delta = 0.17$)
perp-[(OETPP)Fe(1-MeIm)$_2$]$^+$ (73.1°)	0.26 ± 0.02 (4.2 K)	1.94 ± 0.02	−0.85 ± 0.25	$V_{xx} = -1.61$ $V_{yy} = -0.13$ $V_{zz} = 1.74$	$g_{xx} = 1.14$[d] $g_{yy} = 2.00$[d] $g_{zz} = 3.27$[e]	$A_{xx} = -383 \pm 80$ (−358) $A_{yy} = 244 \pm 20$ (174) $A_{zz} = 712 \pm 10$ (714) (crystal field $V/\lambda = 1.16$, $\Delta/\lambda = 3.44$, $V/\Delta = 0.34$)
[(OETPP)Fe(4-Me$_2$NPy)$_2$]$^+$ (70.0°)	0.26 ± 0.02 (4.2 K)	2.13 ± 0.02	−0.63 ± 0.20	$V_{xx} = -1.63$ $V_{yy} = -0.37$ $V_{zz} = 2.00$	$g_{xx} = 0.99$[d] $g_{yy} = 1.96$[d] $g_{zz} = 3.35$[f]	$A_{xx} = -365 \pm 50$ (−351) $A_{yy} = 203 \pm 25$ (201) $A_{zz} = 714 \pm 10$ (761) (crystal field $V/\lambda = 1.02$, $\Delta/\lambda = 3.12$, $V/\Delta = 0.33$)
paral-[(TMP)Fe(5-MeHIm)$_2$]$^+$ (26°, 30°)[86]	0.26 ± 0.02 (4.2 K)	2.59 ± 0.02	−2.22 ± 0.30	$V_{xx} = -2.57$ $V_{yy} = 0.97$ $V_{zz} = 1.59$	$g_{xx} = 1.80$[d] $g_{yy} = 2.30$[d] $g_{zz} = 2.64$[g]	$A_{xx} = -428 \pm 20$ (−455) $A_{yy} = 202 \pm 15$ (124) $A_{zz} = 489 \pm 10$ (314) (crystal field $V/\lambda = 3.10$, $\Delta/\lambda = 4.09$, $V/\Delta = 0.76$)
paral-[(OMTPP)Fe(1-MeIm)$_2$]$^+$ (19.5°)	0.28 ± 0.02 (4.2 K)	2.78 ± 0.02	−2.00 ± 0.20	$V_{xx} = -2.73$ $V_{yy} = 0.91$ $V_{zz} = 1.82$	$g_{xx} = 1.54$[e] $g_{yy} = 2.51$[e] $g_{zz} = 2.71$[e]	$A_{xx} = -438 \pm 50$ (−420) $A_{yy} = 260 \pm 25$ (284) $A_{zz} = 499 \pm 15$ (382) (crystal field $V/\lambda = 2.44$, $\Delta/\lambda = 1.87$, $V/\Delta = 1.31$)
[(TMP)Fe(1-MeIm)$_2$]$^+$ (0°)	0.27 ± 0.02 (4.2 K)	2.24 ± 0.02	−1.85 ± 0.20	$V_{xx} = -2.18$ $V_{yy} = 0.65$ $V_{zz} = 1.53$	$g_{xx} = 1.571$[h] $g_{yy} = 2.325$[h] $g_{zz} = 2.886$[h]	$A_{xx} = -400 \pm 50$ (−417) $A_{yy} = 100 \pm 15$ (187) $A_{zz} = 400 \pm 10$ (465) (crystal field $V/\lambda = 2.07$, $\Delta/\lambda = 3.09$, $V/\Delta = 0.67$)

[a] Axis system of the EFG is taken to be collinear to that of the **g**- and **A**-tensors. [b] *g*-values are a combination of those measured from EPR spectra and those obtained from magnetic Mössbauer spectral fits, as indicated. [c] Values in parentheses are derived from the crystal field model.[84] [d] *g*-values from Mössbauer fit. [e] *g*-values from ref 59. [f] *g*-value from ref 58. [g] *g*-value from ref 55. [h] *g*-values from ref 56.

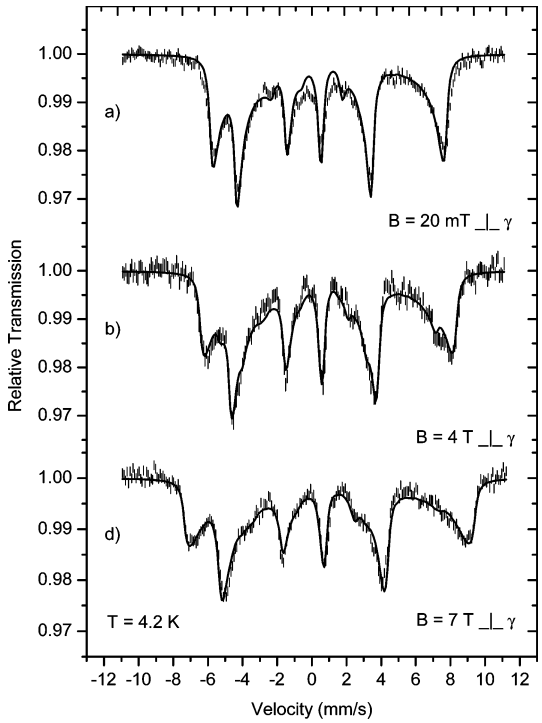

Figure 1. Mössbauer spectra of *perp*-[(OMTPP)Fe(1-MeIm)$_2$]Cl ($\Delta\varphi$ = 90°) obtained at 4.2 K in the presence of several different magnetic fields applied perpendicular to the γ-beam (20 mT (a), 4 T (b), and 7 T (c)). The solid lines are fits performed in the limit of *slow relaxation* with parameters given in Table 1.

corresponding spin expectation value. If the main axis systems of the **g**- and **A**-tensors coincide, then the components of the internal hyperfine field at the ^{57}Fe nucleus are proportional to $\langle S_i \rangle \cdot A_{ii}$, with $i = x, y$, or z, or, if the reference frames of the **g**- and **A**-tensors are collinear, to $g_{ii} \cdot A_{ii}$. Clearly, for *perp*-[(OMTPP)Fe(1-MeIm)$_2$]Cl, both A_{zz} and g_{zz} are the tensor components with the largest magnitude (Table 1). Therefore, the magnetic splitting observed in the Mössbauer spectrum is determined mainly by the product $\langle S_z \rangle \cdot A_{zz}$. Moreover, for all Type I complexes examined thus far, the magnetic splitting is proportional to $g_{ii} \cdot A_{ii}$ because at least the *z*-axes of the reference frames of the **g**- and **A**-tensors coincide.[73] Both A_{xx} and A_{yy} are significantly smaller than A_{zz}. As shown previously,[73] $|A_{zz}| \gg |A_{yy}|$, $|A_{xx}|$ holds for the Mössbauer spectra of all Type I[47] complexes. Thus, for *perp*-[(OMTPP)Fe(1-MeIm)$_2$]Cl in this study (Figure 1, Supporting Information Figure S1, and Table 1), A_{zz} is quite large and positive, A_{yy} is approximately one-third of A_{zz}, and A_{xx} has approximately the same magnitude as A_{yy} and is negative.

In contrast to *perp*-[(OMTPP)Fe(1-MeIm)$_2$]Cl, the low-field spectra (20 mT at 4.2 K) of *perp*-[(OETPP)Fe(1-MeIm)$_2$]Cl ($\Delta\varphi$ = 73.1°) shown in Figure 2a, and [(OETPP)Fe(4-Me$_2$NPy)$_2$]-Cl ($\Delta\varphi$ = 70°), shown in Supporting Information Figure S3a, exhibit broad asymmetric doublets, which indicates that the electron spin fluctuates with a rate, ω, comparable to the Larmor frequency of the iron, $\langle \vec{S} \rangle \cdot \vec{S}/\hbar$, which is of the order of 10^7 s^{-1}. The quadrupole splitting, ΔE_Q, is 1.94 mm/s for *perp*-[(OETPP)-Fe(1-MeIm)$_2$]Cl ($\Delta\varphi$ = 73.1°) and 2.13 mm/s for [(OETPP)-Fe(4-Me$_2$NPy)$_2$]Cl ($\Delta\varphi$ = 70°). The application of high magnetic fields decreases the electronic relaxation rate, and magnetically split patterns are observed (Figure 2b,c and Supporting Information Figure S3). This means that in high magnetic fields the electron spin fluctuates with a rate slower than the Larmor frequency of the iron nucleus. The magnetic splittings observed for *perp*-[(OETPP)Fe(1-MeIm)$_2$]Cl and [(OETPP)Fe(4-Me$_2$NPy)$_2$]Cl are (as in the case of the 90° complex, *perp*-[(OMTPP)Fe(1-MeIm)$_2$]Cl) dominated by A_{zz}. The values of A_{zz} = 712 and 714 kG obtained for these complexes are about 33% smaller than A_{zz} of the 90° complex, *perp*-[(OMTPP)Fe(1-MeIm)$_2$]Cl. The large values of A_{zz} and

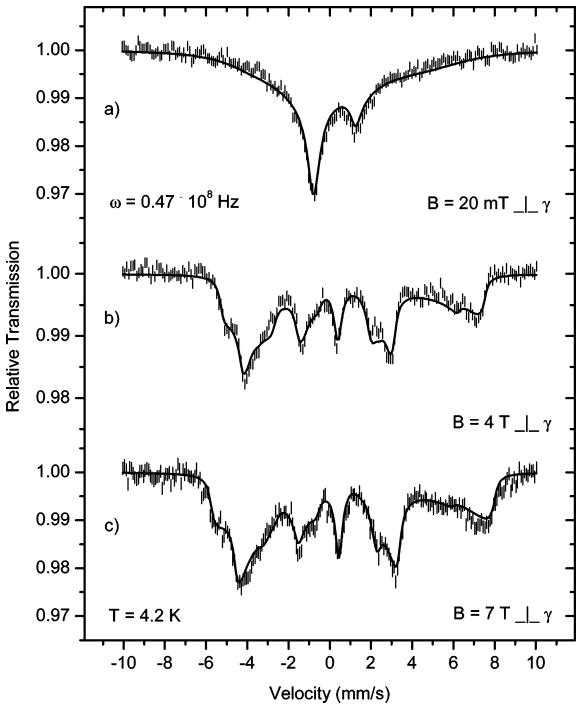

Figure 2. Mössbauer spectra of *perp*-[(OETPP)Fe(1-MeIm)$_2$]Cl ($\Delta\varphi$ = 73.1°) recorded at 4.2 K in the presence of several different magnetic fields applied perpendicular to the γ-beam (20 mT (a), 4 T (b), and 7 T (c)). The solid line in the spectrum recorded at 20 mT (a) is a fit taking *spin−spin relaxation effects* (with relaxation rate $\omega = 0.47 \times 10^8$ Hz) into account,[93] and the other solid lines (4 T (b) and 7 T (c)) are fits performed in the limit of *slow relaxation* with parameters given in Table 1.

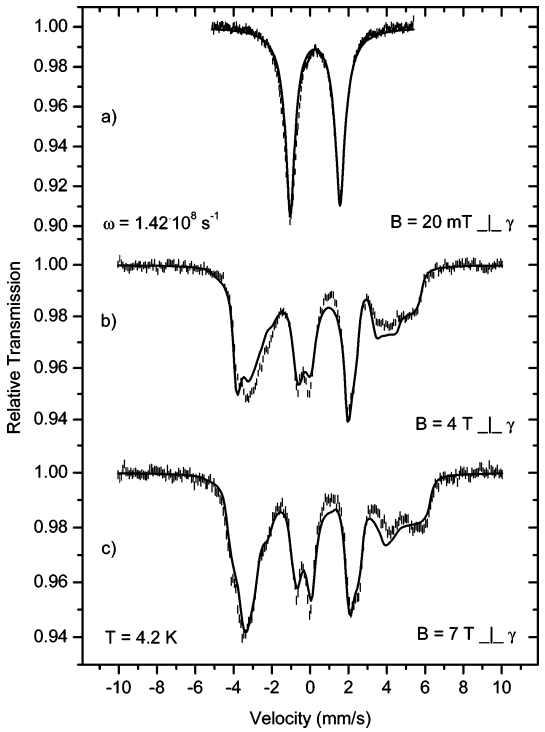

Figure 3. Mössbauer spectra of *paral*-[(TMP)Fe(5-MeHIm)$_2$]ClO$_4$ ($\Delta\varphi$ = 26°, 30°)[86] taken at 4.2 K in the presence of several different magnetic fields applied perpendicular to the γ-beam as indicated. The solid line in the spectrum recorded at 20 mT (a) is a fit taking *spin−spin relaxation effects* (with $\omega = 1.42 \times 10^8$ Hz) into account,[93] while the other solid lines (b and c) are fits performed in the limit of *slow relaxation* with parameters given in Table 1.

g_{zz} and the negative values of A_{xx} are typical of Type I[47] complexes. The asymmetry parameter $\eta \approx -1$ means that the EFG tensor elements for the Type I[47] complexes exhibit a small V_{yy}, while V_{xx} and V_{zz} are of similar magnitude but with a negative value of V_{xx} (Table 1).

Figure 3 shows the Mössbauer spectra of *paral*-[(TMP)Fe(5-MeHIm)$_2$]ClO$_4$ ($\Delta\varphi$ = 26°, 30°).[86] The spectrum obtained at 20 mT (Figure 3a) shows an asymmetric doublet, which indicates that the spin relaxation rate is faster than that of *perp*-[(OETPP)Fe(1-MeIm)$_2$]Cl. The application of large external fields perpendicular (Figure 3b,c) and parallel (Supporting Information Figure S4) to the γ-beam slows the relaxation, and the spectral shape could be well reproduced with the parameters given in Table 1. The quadrupole splitting of this complex is 2.59 mm/s, an increase of approximately 33% as compared to *perp*-[(OETPP)Fe(1-MeIm)$_2$]Cl with ΔE_Q = 1.94 mm/s. The higher value of the quadrupole splitting and the pattern of the magnetic Mössbauer spectra induced by the application of large external fields (Figure 3b,c and Supporting Information Figure S4) are characteristic of most Type II[47] centers.[73] Likewise, [(TMP)Fe(1-MeIm)$_2$]ClO$_4$ ($\Delta\varphi$ = 0°) also shows an asymmetric doublet at 4.2 K in the presence of a 20 mT field (Figure 4a) with ΔE_Q = 2.24 mm/s. The application of large external fields produced the spectra shown in Figure 4b,c and Supporting Information Figure S6, where the spectral shapes were well reproduced with the parameters given in Table 1. The magnetic splitting of the Mössbauer signal of the solid-state, natural-abundance samples of *paral*-[(TMP)Fe(5-MeHIm)$_2$]ClO$_4$ and [(TMP)Fe(1-MeIm)$_2$]ClO$_4$ is significantly smaller (as for other Type II centers[73]) than that of Type I centers (Figure 1 and ref 73). Nevertheless, it is still dominated by $\langle S_z \rangle \cdot A_{zz}$, and the value of A_{zz} (+489 kG) is the same in sign but smaller in magnitude than that of Type I complexes. In this case, the value of A_{xx} is only somewhat smaller in magnitude than that of A_{zz}, but of opposite sign, and A_{yy} is much smaller and positive, as observed previously.[73]

The magnetic field dependence of the Mössbauer spectra of *paral*-[(OMTPP)Fe(1-MeIm)$_2$]Cl ($\Delta\varphi$ = 19.5°) (Figure 5 and Supporting Information Figure S5) is comparable overall to those of *paral*-[(TMP)Fe(5-MeHIm)$_2$]ClO$_4$ ($\Delta\varphi$ = 26°, 30°)[86] and [(TMP)Fe(1-MeIm)$_2$]ClO$_4$ ($\Delta\varphi$ = 0°) (Figure 4 and Supporting Information Figure S6) discussed above. In a low field of 20 mT, no significant magnetic splitting is observed; in fact, the spectrum of *paral*-[(OMTPP)Fe(1-MeIm)$_2$]Cl shows a symmetrical doublet. The application of large external fields induces the magnetic splitting characteristic of Type II complexes.[47,73] As mentioned in the caption to Figure 5, these spectra were analyzed in the *fast-relaxation* limit and yielded a value of $A_{zz} = 499 \pm 15$ kG. Analyzing the 7 T spectra in the slow-relaxation limit yielded A_{zz} = 450 kG, but within that limit it was not possible to find a unique set of parameters that also fit the spectra obtained at 4 T. Therefore, we report only the data obtained from fits in the fast-relaxation limit.

The question arises as to the reason for the different relaxation behaviors of the complexes in this study. Ferriheme centers in proteins, such as the low-spin form of cytochrome P450$_{cam}$,[64] several electron-transfer cytochromes,[65,66] the cytochrome b_6f complex,[41] and the histamine complexes of nitrophorins 2 and 4,[90,91] as well as ^{57}Fe-labeled ferriheme models in frozen solution, including [(TPP)Fe(NH$_2$PzH)$_2$]Cl[71] and *perp*-[(OMTPP)Fe(1-MeIm)$_2$]Cl in this study, exhibit magnetically split

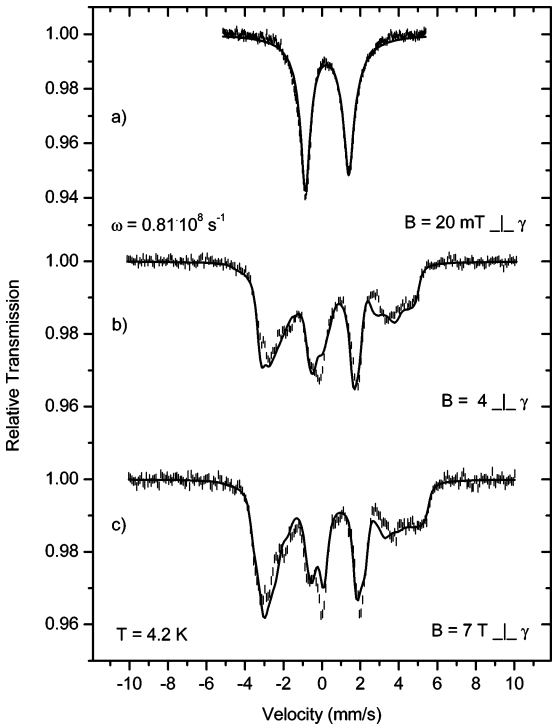

Figure 4. Mössbauer spectra of [(TMP)Fe(1-MeIm)$_2$]ClO$_4$ ($\Delta\varphi$ = 0°) recorded at 4.2 K in the presence of several different magnetic fields applied perpendicular to the γ-beam as indicated. The solid line in the spectrum recorded at 20 mT (a) is a fit taking *spin−spin relaxation effects* (with $\omega = 0.81 \times 10^8$ Hz) into account,[93] while the other solid lines (b and c) are fits performed in the limit of *slow relaxation* with parameters given in Table 1.

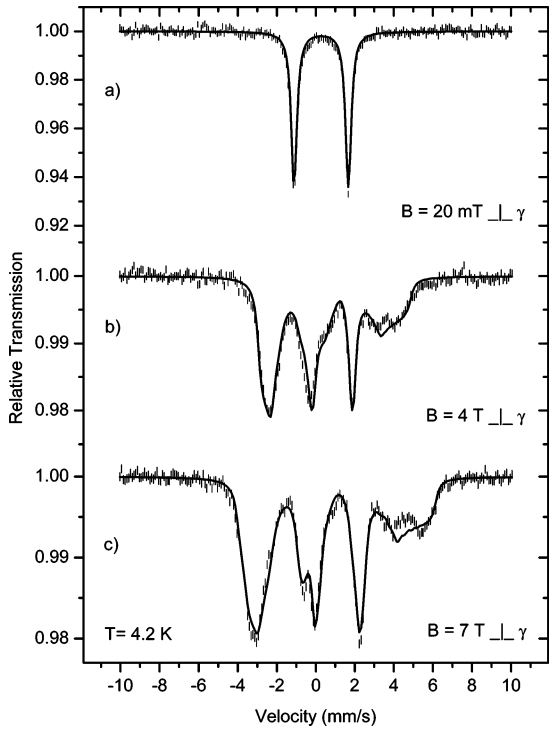

Figure 5. Mössbauer spectra of *paral*-[(OMTPP)Fe(1-MeIm)$_2$]Cl ($\Delta\varphi$ = 19.5°) obtained at 4.2 K in the presence of several different magnetic fields applied perpendicular to the γ-beam as indicated. The solid lines are fits performed in the limit of *fast relaxation* with parameters given in Table 1.

Mössbauer spectra at 4.2 K in small applied fields. This indicates that the intrinsic relaxation rate, ω, of the electron spin of most of these centers is slower than the Larmor frequency, about 10^7 s^{-1}. If the molecules are embedded in a crystal lattice, as in this study, spin−spin relaxation between nearby Fe(III) centers occurs, which increases the relaxation rate of the electron spin. This has also been observed for solid samples of the Type III center [(*p*-TTP)Fe-(2,6-XylylNC)$_2$]CF$_3$SO$_3$,[92] the 4.2 K Mössbauer spectra of which have been analyzed in the intermediate spin−spin-relaxation regime by the dynamic line-shape formalism of Blume and Clauser.[93]

The slow-relaxing 90° complex, *perp*-[(OMTPP)Fe(1-MeIm)$_2$]-Cl, with Type I EPR and Mössbauer spectra, has a unit cell with *I*-43*d* symmetry, in which every molecule has eight nearest iron neighbors at a distance of 12.232 Å, four at 14.620 Å, and eight at 17.906 Å. The fast-relaxing 19.5° complex *paral*-[(OMTPP)Fe(1-MeIm)$_2$]Cl, with Type II EPR and magnetic Mössbauer spectra, has a unit cell with *Pc* symmetry, in which every molecule has two nearest iron−iron distances of 9.54 Å, two of 10.128 Å, and two of 12.15 Å. Thus, the much closer iron−iron distances in *paral*-[(OMTPP)Fe(1-MeIm)$_2$]Cl as compared to *perp*-[(OMTPP)Fe(1-MeIm)$_2$]Cl lead to an increase in the spin−spin relaxation rate, which manifests itself in the observation of a symmetrical doublet in the Mössbauer spectrum at 4.2 K and 20 mT (Figure 5a). The 73.1° sample, *perp*-[(OETPP)Fe(1-MeIm)$_2$]Cl, which exhibits Type I[47] EPR and magnetic Mössbauer spectra (Figure 2b,c), has a unit cell with two nearest iron−iron distances of 12.651 Å and two of 12.86 Å, suggesting that this sample might also exhibit in its Mössbauer spectrum at 4.2 K and 20 mT a relaxation pattern different from the sharp doublet observed for *paral*-[(OMTPP)-Fe(1-MeIm)$_2$]Cl. This is indeed the case; the complex shows intermediate relaxation (Figure 2a), much slower than observed for *paral*-[(OMTPP)Fe(1-MeIm)$_2$]Cl (Figure 5a), but faster than that for *perp*-[(OMTPP)Fe(1-MeIm)$_2$]Cl (Figure 1a). The same is true for the 70° sample, [(OETPP)Fe(4-Me$_2$NPy)$_2$]Cl (Supporting Information Figure S3a), which has two iron−iron distances of 12.245 Å, two of 13.651 Å, and four of 14.052 Å. The remaining two complexes, [(TMP)Fe(5-MeHIm)$_2$]ClO$_4$ ($\Delta\varphi$ = 26°, 30°)[86] and [(TMP)Fe(1-MeIm)$_2$]ClO$_4$ ($\Delta\varphi$ = 0°), both exhibit asymmetric doublets at 4.2 K and 20 mT (Figures 3a and 4a, respectively), but these doublets are much sharper than those for [(OETPP)Fe(4-Me$_2$NPy)$_2$]Cl ($\Delta\varphi$ = 70°, Supporting Information Figure S3a) and *perp*-[(OETPP)Fe(1-MeIm)$_2$]Cl ($\Delta\varphi$ = 73.1°, Figure 2a). Correspondingly, the nearest iron−iron distances (two nearest iron neighbors at 10.670 Å and two at 10.409 Å, respectively) are intermediate between those of *paral*-[(OMTPP)Fe(1-MeIm)$_2$]Cl and *perp*-[(OMTPP)Fe(1-MeIm)$_2$]Cl, as is their relaxation behavior. The correlation between the number of iron neighbors, iron−iron distances, and relaxation behavior of these ferriheme complexes is summarized in Supporting Information Table S1. In each case, the appearance of the 4.2 K, 20 mT Mössbauer spectrum is consistent with a combination of the shortest iron−iron distance and the number of iron neighbors within slightly more than 14 Å. The spin−spin relaxation model applied here does not take into account favorable pathways for electron spin relaxation, which in some cases may also contribute.

The specific structures of *paral*-[(TMP)Fe(5-MeHIm)$_2$]ClO$_4$ ($\Delta\varphi$ = 26°, 30°)[57] and of [(TMP)Fe(1-MeIm)$_2$]ClO$_4$ ($\Delta\varphi$ = 0°),[56] each with two structurally slightly different Fe sites within the unit cell, also allow an alternative interpretation of the asymmetry in the line shapes of the doublets at 4.2 K and 20

Table 2. Mössbauer and EPR Data for Ferriheme Complexes Discussed in This Work and Utilized for Figures 6−8

system	$\Delta\varphi$ (deg)	δ (mm/s)	ΔE_Q (mm/s)	η (kG)	g_{zz}	$A_{xx}/g_N\mu_N$ (kG)	$A_{yy}/g_N\mu_N$ (kG)	$A_{zz}/g_N\mu_N$ (kG)	ref
1 $[(OEP)Fe(4\text{-}Me_2NPy)_2]^+$	0[56]		2.15	−1.8	2.82	−416	−177	446	56
2 $[(TMP)Fe(1\text{-}MeIm)_2]^+$	0[56]	0.27	2.24	−1.85	2.89	−400	100	400	this work
3 bovine cytochrome b_5	19.2[96]				3.03				94
4 *paral*-$[(OMTPP)Fe(1\text{-}MeIm)_2]^+$	19.5[59]	0.27	2.78	−2.00	2.71	−438	260	499	this work
5 rat outer mitochond. memb. cyt b_5	18.2,[97] 23.6[98]				3.03				95
6 NP2-histamine	22−24[108,109]	0.22[a]	2.14	−1.6	3.02	−370	−58	530	90
7 *paral*-$[(TMP)Fe(5\text{-}MeHIm)_2]^+$	26, 30[57,86]	0.26	2.59	−2.22	2.64	−428	202	489	this work
8 NP4-histamine	32[107]	0.19[a]	2.34	−1.6	3.02	−370	−58	540	90
9 murine neuroglobin	59[102]				3.12				99
10 human cytoglobin	60[100,101]				3.20				99
11 $[(OETPP)Fe(4\text{-}Me_2NPy)_2]^+$	70[58]	0.26	2.13	−0.63	3.35	−365	203	714	this work
12 *perp*-$[(OETPP)Fe(1\text{-}MeIm)_2]^+$	73.1[59]	0.26	1.94	−0.85	3.27	−383	244	712	this work
13 $[(TMP)Fe(4\text{-}Me_2NPy)_2]^+$	79[56]		1.75	−1.0	3.44	−331	168	815	56
14 $[(TPP)Fe(2\text{-}MeHIm)_2]^+$	89[51]	0.21[b]	1.71	−2.0	3.41	−347	220	810	39
15 *perp*-$[(OMTPP)Fe(1\text{-}MeIm)_2]^+$	90[59]	0.27	1.70	−0.87	3.61	−225	293	902	this work
16 bovine cytochrome b_H	64[60]				3.41−3.44				38
17 bovine cytochrome b_L	86[60]				3.75−3.78				38
18 cytochrome b_6f heme b_h	67[26,27]	0.30	1.77	0[c]	3.6	−261	−40	926	41
19 cytochrome b_6f heme b_l	83[26,27]	0.30	1.77	0[c]	3.6	−261	−40	926	41

[a] Isomer shift measured at 77 K.[91] [b] Isomer shift measured at 150 K.[39] [c] According to Oosterhuis and Lang,[88] $\eta = -1.8$[73] would be expected in Taylor's formulation[84] for cytochrome b_6. The reported value of $\eta = 0$ suggests an axial EFG tensor, which most probably is not correct. It should be noted that the quality of the experimental data presented in ref 41 and the presence of at least five different iron species did not allow a more precise determination of η by Mössbauer spectroscopy.

mT (Figures 3a and 4a, respectively): A superposition of two slightly different quadrupole splittings, each with symmetric line intensities and therefore each representing fast relaxation, also accounts for the observed asymmetric line patterns in Figures 3a and 4a. These fits are shown in Supporting Information Figures S7 and S8, together with the quadrupole splittings and isomer shifts of the two components used for the fits. Within this alternative model for fitting asymmetric quadrupole doublets, the group of complexes with $\Delta\varphi = 0°$, 19.5° and 26°, 30° exhibit fast relaxation at 4.2 K and 20 mT, the two complexes with $\Delta\varphi = 70°$ and 73.1° exhibit intermediate relaxation, and the complex with $\Delta\varphi = 90°$ exhibits slow relaxation. In summary, we note that, in either of the two fitting procedures, the relaxation process changes from fast relaxation for small angles $\Delta\varphi$ to intermediate relaxation for intermediate values of $\Delta\varphi$ and to slow relaxation for $\Delta\varphi = 90°$.

Unlike the observation for previous powdered samples of low-spin Fe(III) porphyrinates investigated by this group,[73] the magnetic Mössbauer spectra of ground crystals of both *paral*- and *perp*-[(OMTPP)-Fe(1-MeIm)$_2$]Cl exhibit no contamination due to high-spin Fe(III), low-spin Fe(II), or other low-spin Fe-(III) forms of either complex, and the spectra of each of the six complexes of this study could be fit with only one component. This is probably due to the fact that all molecules in the sample have the same axial ligand plane orientations, whereas the previous samples,[73] including those rapidly precipitated solid materials of possibly mixed crystalline forms as well as all frozen solution ^{57}Fe-enriched samples, undoubtedly had a distribution of axial ligand plane dihedral angles. As shown below, in this work we find correlations between the axial ligand plane dihedral angle, $\Delta\varphi$, and the values of g_{zz}, A_{zz}, and ΔE_Q, and thus it is not surprising that the magnetic Mössbauer spectra of polycrystalline or frozen solution samples, which probably have a distribution of axial ligand plane dihedral angles, are not as easily fit.

The detailed results obtained in this work from the careful fitting of Mössbauer spectra in low (20 mT) and high (4.0 and 7.0 T) magnetic fields applied parallel and perpendicular to the direction of the γ-beam for the six bis-imidazole and bis-pyridine complexes of Fe(III) OETPP, OMTPP, and TMP are given in Table 1. In Table 2, the results of this study are summarized, along with EPR and magnetic Mössbauer data of other model heme complexes that were also acquired on the same crystalline form as used for the structure determinations; magnetic Mössbauer data acquired for the histamine complexes of nitrophorins 2 and 4[90] are also included, as are available EPR and structural data for cytochromes b_5,[94−98] cytoglobin,[99−101] and neuroglobin[99,102] and EPR[38,41] and Mössbauer[41] data for the bc_1 and b_6f protein complexes. As can be seen, the three "parallel" model ferriheme complexes have much larger quadrupole splittings than do the three "perpendicular" complexes. This result is consistent with previous studies[39,56,73] and is expected because the "parallel" complexes, with large rhombicity, should have much more asymmetric electron distributions than do the "perpendicular" complexes. Indeed, the "parallel" complexes show an asymmetry parameter $\eta \approx -2$, which means that by far the largest-magnitude component of the EFG, V_{xx}, is much larger than V_{zz}. The "perpendicular" complexes, on the other

(90) Wegner, P.; Benda, R.; Schünemann, V.; Trautwein, A. X.; Berry, R. E.; Balfour, C. A.; Wert, D.; Walker, F. A. *Proceedings of the International Conference on the Applications of the Mössbauer Effect (ICAME 2001), Hyperfine Interact. C* **2002**, *5*, 253−256.
(91) Wegner, P. Ph.D. dissertation, Universität zu Lübeck, 2004.
(92) Simonneaux, G.; Schünemann, V.; Morice, C.; Carel, L.; Toupet, L.; Winkler, H.; Trautwein A. X.; Walker, F. A. *J. Am. Chem. Soc.* **2000**, *122*, 4366−4377.
(93) Clauser, M. J.; Blume, M. *Phys. Rev. B* **1971**, *3*, 583−591.
(94) Bois-Poltoratsky, R.; Eherenberg, A. *Eur. J. Biochem.* **1967**, *2*, 361−365.
(95) Rivera, M.; Barillas-Mury, C.; Christensen, K. A.; Little, J. W.; Wells, M. A.; Walker, F. A. *Biochemistry* **1992**, *31*, 12233−12240.
(96) Durley, R. C. E.; Mathews, F. S. *Acta Crystallogr. Sect. D* **1996**, *52*, 65.
(97) Rivera, M.; Seetharaman, R.; Girdhar, D.; Wirtz, M.; Zhang, X.; Wang, X.; White, S. *Biochemistry* **1998**, *37*, 1485−1494.
(98) Wirtz, M.; Oganesyan, V.; Zhang, X.; Studer, J.; Rivera, M. *Faraday Discuss. Chem. Soc.* **2001**, *116*, 221−234.
(99) Vinck, E.; Van Doorslaer, S.; Dewilde, S.; Moens, L. *J. Am. Chem. Soc.* **2004**, *126*, 4516−4517.
(100) de Sanctis, D.; Dewilde S.; Pesce, A.; Moens, L.; Ascenzi, P.; Hankeln, T.; Burmester, T.; Bolognesi, M. *J. Mol. Biol.* **2004**, *336*, 917−927.
(101) Sugimoto, H.; Makino, M.; Sawai, H.; Kawada, N.; Yoshizato, K.; Shiro, Y. *J. Mol. Biol.* **2004**, *339*, 873−885.
(102) Vallone, B.; Nienhaus, K.; Brunori, M.; Nienhaus, G. U. *Proteins: Struct., Funct. Bioinf.* **2004**, *56*, 85−94.

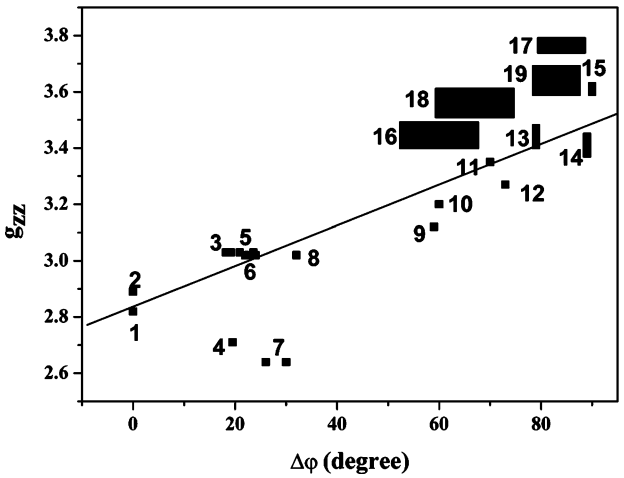

Figure 6. Correlation of g_{zz} with dihedral angle of the axial ligand planes, $\Delta\varphi$. Denotation of the complexes is given in Table 2. Normal rhombic ferriheme signals have fairly sharp EPR signals with g_{zz} measurable to ± 0.01, which is within the size of the square data points, while large g_{max} ferriheme centers often have broad signals, which are represented in this figure as a range of *g*-values for complexes **13**, **14**, and **15**. The correlation line represents the least-squares slope for the model heme complexes, except for **4** and **7**, which are not included in the calculation for reasons discussed in the text. For the bovine bc_1 complex, a range of *g*-values have been reported for each of the cytochrome *b* hemes,[37,38,63] and a range of dihedral angles are also observed.[13,14,17−19,21,22,24,25,60] Hence the data are represented as large blocks for **16** and **17**. For chloroplast cytochrome b_6 hemes (**18**, **19**), Mössbauer spectra yielded $g_{zz} = 3.6$ for both b_h and b_l,[41] but it is possible that the two have somewhat different *g*-values, and again, a range of angles is also found,[26−29] as indicated by the blocks shown for each.

hand, show $\eta \approx -1$, which means that the magnitudes of V_{xx} and V_{zz} are similar.

The isomer shifts of the six complexes are within experimental error of each other and equal to 0.27(2) mm/s, as is expected for low-spin Fe(III) complexes at 4.2 K. The hyperfine coupling constants of the complexes are also consistent with those reported previously,[39,56,73] with the largest-magnitude hyperfine coupling constant, A_{zz}, being considerably smaller for the "parallel" complexes (400−540 kG) than for the strictly perpendicular complex (902 kG), A_{xx} being negative for all six complexes and smallest in magnitude for the strictly perpendicular complex (−225 kG), and A_{yy} being small and usually positive but difficult to estimate with accuracy for all six complexes.

The structure, EPR, and Mössbauer data for bis-imidazole- and bis-pyridine-coordinated OETPP-, OMTPP-, and TMPFe(III) complexes under study in this work,[39,56,90] as well as other well-characterized systems reported previously, allow us to establish for the first time some interesting qualitative correlations of the values of g_{zz}, A_{zz}, or ΔE_Q with the dihedral angle between the axial ligands. In Figure 6 the values of g_{zz} are plotted as a function of the dihedral angle, $\Delta\varphi$, and a linear correlation is observed: g_{zz} increases with increasing $\Delta\varphi$. The g_{zz}-values of the bovine cytochrome bc_1 hemes b_H and b_L and spinach chloroplast cytochrome b_6f hemes b_h and b_l are also included in Figure 6 (data points **16**−**19**, respectively). All these g_{zz} values deviate somewhat from the least-squares fit of the model heme data points. Part of this deviation might be a result of the difference between the substituents present on the natural heme (protohemin IX, heme *b*) and those used for the present study, all of which have phenyl substituents on the *meso*-carbons. However, the nitrophorin (**5** and **8**), cytochrome b_5 (**3** and **6**), neuroglobin (**9**), and cytoglobin (**10**) data points do not deviate significantly from the best-fit line, even though they all also contain heme *b*. Preliminary DFT calculations[103] indicate no obvious dependence of Mössbauer parameters upon heme substituents. More likely, it should be noted that the g_{max} signal for one of the *b* ferrihemes of the bc_1 complex (b_H), as well as those of several of the model ferrihemes (notably **13**,[56] **14**,[51] and to a lesser extent **15**[59]), is broad, probably in part as a result of *g*-strain[104] and in part as a result of a distribution of *g*-values arising from a degree of microheterogeneity in the structures of these ferriheme centers.[38] For the bc_1 complex a range of *g*-values has been reported for each of the *b* ferrihemes (3.41−3.44[38] and as high as 3.48[63] for ferriheme b_H and 3.75−3.78 for ferriheme b_L[38]); the *g*-value reported for the two *b* hemes of cytochrome b_6f is an estimate based upon Mössbauer data,[41] and it is possible that the individual values differ somewhat from this average. Therefore, in Figure 6 we have shown distributions of g_{zz} values for both types of cytochrome *b* heme centers and three of the model ferriheme complexes that have broad "large g_{max}" signals as well.

The maximum possible *g*-value for a low-spin Fe(III) complex is about 3.8,[38] and the ferriheme center of mitochondrial cytochrome b_L (**17**) approaches that limit more closely than any other bis-imidazole-coordinated ferriheme complex currently known; at present we do not know why the model ferrihemes with 89° (**14**) or 90° (**15**) dihedral angles do not have larger g_{max} values.

One possible difference between the model ferrihemes and the large protein complexes is the electrostatic nature of the medium, a concentrated crystal lattice with closely spaced cations and anions as compared to a generally hydrophobic intermembrane location for the cytochrome *b* ferrihemes. However, the latter do have one arginine guanidinium side chain hydrogen-bonded to one of the two propionates of each heme *b*[11−25] (except for yeast b_H, where a lysine ammonium side chain plays this role[21−24]), thus making the protohemin center neutrally charged overall, and isolated by nearly 10 Å between the heme edges of b_L and b_H or b_l and b_h, or 20.2−20.9 Å between Fe(III) centers.[11−25] As already mentioned above, in the crystalline model complexes of this study the closest distances between Fe(III) centers range from 9.5 to 12.7 Å, depending on crystal form (Supporting Information Table S2). How to evaluate the possible contributions of the difference in electrostatic medium and/or greater distances between iron centers to the observed EPR *g*-values is not clear at this time.

The two synthetic complexes of the present study whose values of g_{zz} deviate the most from the best-fit line of Figure 6 have special structural features that may contribute to the deviation of their *g*-values from the least-squares line for the other model ferriheme complexes. Complex **7**, *paral*-[(TMP)Fe(5-MeHIm)$_2$]$^+$, has one 5-MeHIm ligand N−H hydrogen-bound to a lattice 5-MeHIm, and the other 5-MeHIm ligand N−H hydrogen-bound to an oxygen of the perchlorate anion, both of which make the bound ligands more imidazolate-like (frozen solution samples yielded *g*-values of 2.89, 2.31, and 1.58 for an Fe to 5-MeHIm ratio of ∼1:2. but 2.64, 2.30, and 1.80 for a ratio of 1:60, where sufficient excess 5-MeHIm is

(103) Teschner, T.; Paulsen, H.; Schuenemann, V.; Walker, F. A.; Trautwein, A. X. Unpublished work.
(104) De Vries, S.; Albracht, S. P. J. *Biochim. Biophys. Acta* **1979**, *546*, 334−340.

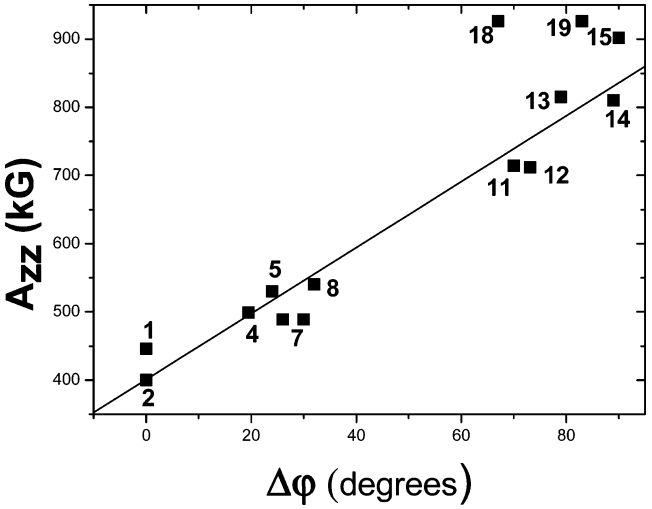

Figure 7. Correlation of A_{zz} with the dihedral angle between the axial ligand planes, $\Delta\varphi$. In all cases the error in the fitted value of A_{zz} is 10 kG or less (Table 1), as represented by the sizes of the square data points. Denotation of the complexes is given in Table 2. The data points for chloroplast cytochrome b_6 (**18**, **19**) are not included in calculation of the least-squares line for reasons discussed in the text.

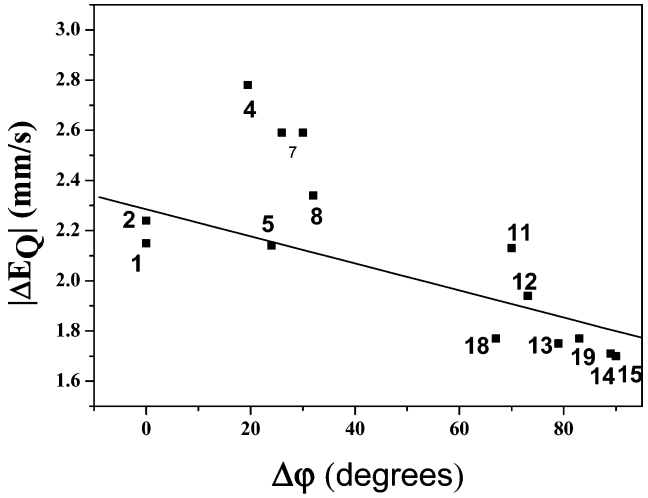

Figure 8. Correlation of ΔE_Q with dihedral angle of the axial ligand planes. In all cases the error in the fitted value of ΔE_Q is $\pm$0.02 mm/s (Table 1), and thus falls within the sizes of the square data points. Denotation of the complexes is given in Table 2. Data points **4**, **7**, **18**, and **19** are not included in the calculation of the least-squares line for reasons discussed in the text.

available to act as hydrogen bond acceptors from the bound 5-MeHIm ligands).[57] Complex **4**, *paral*-[(OMTPP)Fe(1-MeIm)$_2$]$^+$, has one Fe−N axial ligand bond significantly longer than the other (2.0155(19) as compared to 1.9747(19) Å) and longer than for other low-spin iron(III) porphyrinates, with the shorter-bonded ligand being farther off the heme normal (9.1°) than the longer-bonded ligand (3.2°).[59] The *g*-values of these two model ferriheme complexes, as well as the cytochrome *b* and b_6 *g*-values, have not been included in the calculation of the least-squares line because of these structural features.

The correlation is better for the plot of A_{zz} against $\Delta\varphi$ shown in Figure 7, except for the cytochrome b_6 data points (**18**, **19**); the deviation of the latter is mainly a consequence of the difficulty of fitting the magnetic Mössbauer spectra of complex systems consisting of overlapping broad spectra (three in the cytochrome b_6f case). The fact that both g_{zz} and A_{zz} are correlated with the dihedral angle $\Delta\varphi$ is not surprising, because a correlation exists between A_{zz} and g_{zz}.[73] Thus, it is a bit surprising that point **4** does not fall off the best-fit line of the plot of A_{zz} vs $\Delta\varphi$, as it does for the plot of g_{zz} (and also ΔE_Q, discussed below) vs $\Delta\varphi$. In the case of **4**, it is possible that this discrepancy might be a result of the choice of the fast-relaxation limit for analysis of the magnetic Mössbauer data. This choice is justified by the fact that we observe a symmetric doublet with no magnetic splitting at 4.2 K in a field of 20 mT (Figure 5a). Nevertheless, we have also analyzed the 7 T spectra of **4** in the slow-relaxation limit, which reduces A_{zz} from 499 to 450 kG. However, within this limit of slow relaxation it was not possible to find a unique parameter set that also fits the spectra obtained at 4 T. Therefore, we have reported the fast-relaxation limit fit for **4** in Table 1 and Figure 7. Although the slow-relaxation limit value of 450 kG would cause this data point to be off the correlation line, it would still deviate less than do data points **1** and **15**. Despite the deviations, utilizing the correlations between $\Delta\varphi$ and g_{zz} or A_{zz}, we have a new method for obtaining structural information. By using Figures 6 and 7, unknown dihedral angles of ferriheme axial ligands may be roughly estimated by measuring g_{zz} by EPR spectroscopy and/or (preferably) A_{zz} by Mössbauer spectroscopy.

A linear correlation between ΔE_Q and $\Delta\varphi$ is less obvious (Figure 8), although in general Type I[47] complexes with $\Delta\varphi \geq 70°$ show ΔE_Q less than or approximately equal to 2.1 mm/s, and Type II[47] complexes have ΔE_Q values in the range from 2.2 to as large as 2.8 mm/s. We have checked to see whether off-axis binding of axial ligands, or small vs large angles between axial ligands and the N−Fe−N porphyrin axes, may affect the Mössbauer parameters obtained, but from the data summarized in Supporting Information Table S2, no dependence of the parameters on these factors is obvious. The largest deviations from the plots of g_{zz} and ΔE_Q (there are no large deviations from the plot of A_{zz}) vs axial ligand plane dihedral angle, $\Delta\varphi$, are for **4** (*paral*-[(OMTPP)Fe(1-MeIm)$_2$]$^+$) and **7** (*paral*-[(TMP)Fe(5-MeHIm)$_2$]$^+$), and while **4** does have a large deviation of one ligand from the heme normal (9.1°), **7** does not (4.0° and 6.8° for one ligand of each of the two molecules in the unit cell of **7**). The largest deviations from the heme normal (10°, 12°; 10.6°; and 12.2°) are exhibited by **8** (NP4-histamine), **14** ([(TPP)Fe(2-MeHIm)$_2$]$^+$, and **11** ([(OETPP)Fe-(4-Me$_2$NPy)$_2$]$^+$), respectively, for which the correlations of g_{zz} and ΔE_Q with $\Delta\varphi$ do not deviate significantly from the least-squares lines (Figures 6 and 8).

Thus, the Mössbauer and EPR parameters for bis-imidazole and bis-pyridine Fe(III) porphyrinates of this study, as well as those of other $(d_{xy})^2(d_{xz},d_{yz})^3$ ground-state systems included in Table 2 and Figures 6−8, are part of a continuum that appears to exist for Type I and Type II complexes, except that so far there are no Mössbauer data for complexes having axial ligand plane dihedral angles between 30° and 70°. The recent solution of three structures of [(OETPP)FeL$_2$]$^+$ complexes, where L = imidazole, 1-benzylimidazole, and 1-methylimidazole, however, appears to fill that gap with molecules having ligand plane dihedral angles ranging from 16.0° to 30.3° to 44.6° to 56.8° to 57.2° to 59.6° to 88.1°.[105] The smallest four dihedral angle centers give rise to normal rhombic EPR spectra, while the

(105) Yatsunyk, L. A.; Dawson, A.; Carducci, M. D.; Walker, F. A. *J. Am. Chem. Soc.*, in press.

largest three dihedral angle centers give rise to "large g_{max}" EPR spectra.[105] From this group of molecular structures, it thus appears that the transition from normal rhombic to "large g_{max}" is sharp and occurs at an axial ligand plane dihedral angle of 57°.[105] However, no Mössbauer spectra have yet been obtained on these new crystalline forms to allow us to evaluate trends in A_{zz} and ΔE_Q.

From the present study, we can reach conclusions about the extremes in axial ligand plane dihedral angles, from 0° to 30° and 70° to 90°. The *perp*-[(OMTPP)Fe(1-MeIm)$_2$]Cl ($\Delta\varphi$ = 90°) has a value of A_{zz} that is among the largest reported thus far for bis-histidine-coordinated heme centers[73] and similar to those of cytochrome b_6 of chloroplasts,[41] heme *c* of *Thiobacillus denitrificans* cytochrome cd_1 nitrite reductase,[68] and low-spin heme *c*(1) of *Desulfovibrio desulfuricans* hexaheme nitrite reductase[70] (926, 910, and 926 kG, respectively). *paral*-[(TMP)Fe(5-MeHIm)$_2$]ClO_4, *paral*-[(OMTPP)Fe(1-MeIm)$_2$]Cl, and [(TMP)Fe(1-MeIm)$_2$]ClO_4 have values of A_{zz} that are typical of complexes known to have axial ligands in strictly or at least nearly parallel planes, including [(OEP)Fe(4-Me$_2$NPy)$_2$]ClO_4,[56] [(OEP)Fe(1-MeIm)$_2$]ClO_4,[72] [((((OMe)$_2$)$_4$TPP)Fe(1-MeIm)$_2$]$^+$,[73] and [((((OMe)$_2$)$_4$TPP)Fe(4-NMe$_2$Py)$_2$]$^+$ [73] among model hemes (446, 550, 530, and 500 kG, respectively, all of which represent best fits to frozen solution ^{57}Fe-labeled samples which probably consisted of distributions of "parallel" ligand planes) and low-spin hemes *c*(4) and *c*(5) of *D. desulfuricans* hexaheme nitrite reductase[70] (540 and 505 kG, respectively) and nitrophorins 2 and 4 (530 and 540 kG, respectively[90])[106−109] among heme proteins. It would be interesting to carry out a magnetic Mössbauer spectroscopic investigation of mitochondrial Complex III, but because the cytochrome bc_1 complex contains three heme centers, all with "large g_{max}" EPR signals,[38] deconvolution of the three overlapping spectra, likely with similar values of A_{zz}, would be extremely difficult without using redox poising of several Mössbauer samples, as has been done to deconvolute the EPR signals,[38] and even then there would still be spectral overlap, as was true in the case of the Mössbauer spectra of chloroplast b_6f.[41]

(106) The crystal structure of nitrophorin 4 (NP4), bound to the imidazole nitrogens of histidine-59 and exogenous histamine (Hm), has been solved and shown to have an imidazole plane dihedral angle of 32°.[107] Likewise, detailed ^{1}H and ^{13}C NMR investigations have shown that the imidazole plane dihedral angle for the histamine complex of NP2 is 22−24°.[108,109]

(107) Roberts, S. A.; Weichsel, A.; Qin, Y.; Shelnutt, J. A.; Walker, F. A.; Montfort, W. R. *Biochemistry* **2001**, *40*, 11327−11337.

(108) Shokhireva, T. Kh.; Shokhirev, N. V.; Walker, F. A. *Biochemistry* **2003**, *42*, 679−693.

(109) Shokhireva, T. Kh.; Smith, K. M.; Andersen, J. F.; Weichsel, A.; Balfour, C.; Montfort, W. R.; Walker, F. A. To be submitted.

Conclusions

We have shown for the first time that relationships exist between increasing dihedral angle of the axial ligand planes, $\Delta\varphi$ (from 0° to 90°), and EPR and Mössbauer spectroscopic properties. A_{zz} dominates the magnetic splitting of the Mössbauer spectra exhibiting "large g_{max}" EPR signals (Type I complexes). The values of g_{zz} and A_{zz} increase with increasing dihedral angle (Figures 6 and 7), which means that the hyperfine field $\mathbf{B}_{hf}$ is greatest for perpendicular ligand plane orientation. In contrast, the quadrupole splitting behaves oppositely, decreasing with growing dihedral angle (Figure 8). In general, the "parallel" complexes show asymmetry parameters η near −2, which means that the largest-magnitude component of the EFG, V_{xx}, is much greater than V_{zz}, while the "perpendicular" complexes show η near −1, which means that the magnitudes of V_{xx} and V_{zz} are similar. Thus, an increasing dihedral angle of the ligand planes leads to a smaller distortion of the charge density at the iron center.

Acknowledgment. We thank the National Institutes of Health, Grant DK-31038 (F.A.W.) and Grant GM-38401 (W.R.S.), and the Deutsche Forschungsgemeinschaft (A.X.T.) for support of this research. This paper was written while F.A.W. was on sabbatical leave in the Institut für Physik, Universität zu Lübeck, with support from an Alexander von Humboldt Senior Award in Science, and is dedicated to Prof. Philipp Gütlich on the occasion of his 70th birthday.

Supporting Information Available: Additional Mössbauer spectra of complexes (Figures S1−S8), iron−iron distances in the six crystalline solids (Table S1), and ligand deviations from the normal to the mean porphyrin plane and ligand plane orientations with respect to the N−Fe−N axes for the complexes of this study (Table S2). This material is available free of charge via the Internet at http://pubs.acs.org.

JA056343K